Journal of Science-FAS-SEUSL (2025) 06(02) 115-122
ISSN:2738-2184

The Study of the role of CuSCN and Spiro-OMETAD in the hole transport of Sb_2S_3 solar cells

M.A. Farhana[a] and J. Bandara[b*]

[a]Department of Physical Sciences, Faculty of Applied Sciences, South Eastern University of Sri Lanka, Sammanthurai, Sri Lanka 32200
[b]National Institute of Fundamental Studies, Hantana Road, Kandy, Sri Lanka 20000

[*]jayasundera.ba@nifs.ac.lk

Abstract:
In this study, we systematically examine Sb_2S_3 solar cells featuring CuSCN and Spiro-OMETAD as hole-transport layers (HTLs) across four different configurations, such as a single layer of CuSCN (FTO/TiO_2/Sb_2S_3/CuSCN/Ag), a bilayer of CuSCN/Spiro (FTO/TiO_2/Sb_2S_3/CuSCN/Spiro/Ag), a bilayer of Spiro/CuSCN (FTO/TiO_2/Sb_2S_3/Spiro/ CuSCN/Ag), and a single layer of Spiro (FTO/TiO_2/Sb_2S_3/Spiro/Ag). Photovoltaic performance of the cells showed the highest power conversión efficiency (PCE) for a single layer of Spiro and followed by a bilayer of CuSCN/Spiro, a single layer of CuSCN, and a bilayer of Spiro/CuSCN. Due to the optimal energy level alignment and interface resistance of Spiro and Sb_2S_3, superior performance was obtained compared to other configurations. Architecture employing CuSCN exclusively delivered competitive power conversión efficiency consistent with reported favourable properties in solar cells. Introducing a CuSCN interlayer beneath Spiro yielded slightly low performance, while CuSCN at the top of Spiro yielded inferior performance. By carefully engineering bilayer stacks, the strength of both materials can be harnessed effectively without introducing interfacial impediments, and high-efficiency Sb_2S_3 photovoltaic designs.

Keywords: Bilayer, HTLs, Interface

1. Introduction

Solar cell technology is a key component in the transition to sustainable energy sources because of its versatility and scalability. The first solar cell was invented with a power conversion efficiency of just 1%, whereas current commercialised solar cells typically exhibit an efficiency of above 23% [1-2]. This explores a significant progress in solar cell technology. These commercial solar cells can be classified into four types: monocrystalline, polycrystalline, thin films, and passivated emitter and rear cell (PERC) solar panels. Monocrystalline solar panels are made from single-crystal silicon solar cells, while polycrystalline ones consist of multiple silicon fragments that are melted and poured. Both types have achieved top efficiencies of 23-26%. Thin-film solar cells are hundreds of times thinner than other solar panels, which makes them more flexible and lightweight. Different types of thin film solar panels include amorphous silicon, cadmium telluride (CdTe), and copper indium gallium selenide (CIGS), which have recently reached maximum efficiencies of 14%, 22.6%, and 23.6%, respectively [3].

Since solid-state solar cells simplify manufacturing and enhance durability, researchers are actively working to introduce new materials to address the scarcity and toxicity of traditional

Corresponding Author: jayasundera.ba@nifs.ac.lk

materials, such as CIGS and CdTe. Among the various components of solar cells, the front and back contacts, active material (absorber), and electron and hole transport layers are fundamental. Since the charge extraction is one of the crucial features, the Hole Transport Materials (HTMs) are widely investigated in solar cells. These HTMs are used to prevent the undesired charge recombination at the interface and facilitate the charge transaction. Consequently, our study examined the development of incorporating HTMs between Sb_2S_3 and the front contact, with Sb_2S_3 serving as the active layer (light absorber). Although some research has been conducted without HTMs, the efficiency remains lacking.

2. Literature Review

The amorphous nature, good conductivity with dopants, and high melting point of spiro-OMeTAD make it one of the most adaptable HTMs. Since pristine spiro-OMeTAD has relatively low hole mobility (10^{-4}-10^{-5} cm^2 V^{-1} s^{-1}) and low conductivity, it exhibits poor performance. Therefore, spiro-OMeTAD is prepared by doping with LiTFSI and tBP [4-5]. These types of organic HTMs are widely used for their high efficiency in solar cells. However, the organic materials are much expensive compared to inorganic materials also require complex synthesis. Due to the high hole mobility (0.01-0.1 cm^2 V^{-1} s^{-1}) and thermal stability, CuSCN is an extensively studied inorganic compound in solar cell applications as a HTM [6-7]. Since this resource is abundant and relatively inexpensive, the fabrication cost can be reduced. In recent years, CuSCN has been widely used in perovskite solar cells and solid-state dye-sensitized solar cells (SSDSSC). Moreover, numerical studies of CuSCN as a HTM show that with a particular architecture, efficiency can reach 25% in perovskite solar cells [8] and 17% in SSDSSC [9]. Therefore, we used CuSCN and spiro as HTMs in this study to evaluate the Sb_2S_3 solar cells.

3. Methodology

3.1 Preparation of TiO_2 layer

A mixture of 50 µl of di-ethanolamine and 910 µl of butan-1-ol was stirred for 10 minutes. Then, 75 µl of TTIP was added to the above mixture to prepare a clear precursor solution of 0.25 mM TiO_2. The prepared solution was spin-coated on the cleaned FTO glass at 3000 rpm for 30 s. The TiO_2 layer was fabricated with four spinning cycles. After every spinning cycle, the TiO_2 films were heated on the hot plate at 180 ^oC for 5 minutes. Finally, TiO_2 was sintered inside the furnace at 500 ^oC for 1 hour with 1 1-hour ramp and followed the natural cooling. They were used as an electron transport layer in our solar devices.

3.2 Preparation of active (Sb_2S_3) layer

114 mg of thiourea (TU) was mixed with 1 ml of 2-methoxyethanol and stirred until completely dissolved. Then, 228 mg of $SbCl_3$ was added to the TU solution and stirred for 30 minutes. The precursor solution was spin-coated at 4000 rpm for 30 s on the TiO_2 layer. It was heated inside the tube furnace at 180 °C for 1 min and followed by annealing inside the tube furnace at 280 °C for 10 minutes under N_2 gas.

3.3 Preparation of hole transport layer

A 20 mg of CuSCN was dissolved in 1 ml of 2-Ethylsulfide to prepare the CuSCN solution. Then, the Spiro solution was prepared by using 3.6 mg of Spiro-OMeTAD in 100 μl of chlorobenzene, 1.0 μl of Li+ solution, and 1.5 μl of TBP. The Li+ solution was prepared by adding 520 mg of bis (trifluoromethane sulfonyl) imide lithium salt to 1 ml of acetonitrile. The prepared solutions of the above CuSCN and Spiro were spin-coated on Sb_2S_3 at 3000 rpm for 30 s. The coated cells were heated on the hot plate at 100 ^oC for 20 minutes.

3.4 Counter electrode preparation

Finally, 70 nm of silver (Ag) layer was deposited by the thermal evaporation technique.

3.5 Cell assembly

The following sets of cells were fabricated separately.

i. FTO/TiO_2/Sb_2S_3/CuSCN/Ag;
ii. FTO/TiO_2/Sb_2S_3/CuSCN/Spiro/Ag;
iii. FTO/TiO_2/Sb_2S_3/Spiro/CuSCN /Ag;
iv. FTO/TiO_2/Sb_2S_3/Spiro/Ag

3.6 Characterizations

The cells were fabricated with an effective area of 0.18 cm^2. Current–Voltage measurements and EIS were done of each cell using Metrohm Autolab under the illumination of 100 mW cm^{-2} with AM 1.5 spectral filter. IPCE curves were measured as a function of wavelength from 300 nm to 800 nm using the Bentham PVE300 photovoltaic Device Characterization System.

4. Results and Discussion

4.1 Current Density-Voltage (J-V) analysis

Figure 1 presents the J-V characteristic curves of the devices with various HTM configurations, and photovoltaic parameters, including short circuit current density (Jsc), open circuit voltage (Voc), fill factor (FF), and power conversion efficiency (PCE) are summarized in Table 1. The cell of FTO/TiO_2/Sb_2S_3/Spiro/CuSCN/Ag showed poor performance, while FTO/TiO_2/Sb_2S_3/Spiro/Ag demonstrated superior performance. The cell with Spiro reached a PCE of 3.72%, with a Jsc of 14.9 mA cm^{-2}, Voc of 585.6 mV, and a fill factor of 42.6%. This efficiency was nearly 16 times greater than the cell of FTO/TiO_2/Sb_2S_3/CuSCN/Ag. The electronic properties of Spiro and CuSCN are illustrated in Table 2. It was noted that photogenerated holes quickly localize on sulfur atoms in Sb_2S_3, creating sulfide radical species. A two-step hole injection was noted across the Sb_2S_3/CuSCN interface. It was indicated by the exponential time constant of the transfer of the trapped holes to CuSCN [10]. However, the formation of large CuSCN crystals impedes the efficiency of hole transfer, leading to a poor interfacial contact and increased recombination losses. Additionally, the hole extraction can be hindered by the defect at the CuSCN/Sb_2S_3 interface, which reduces the device performance.

The material with high hole mobility reduces losses during hole transport. But, the interface of Sb_2S_3/CuSCN in solar cells exhibits a lower hole extraction than the electron extraction. Therefore, most of the holes are laying in Sb_2S_3, which leads to the recombination at TiO_2/Sb_2S_3. Hence, due to the poor hole transfer, the cell reached low efficiency with CuSCN. For the effective extraction of holes, the lowest unoccupied molecular orbital (LUMO) level of HTM must be well-matched with the LUMO level of the acceptor (Sb_2S_3) to minimize charge injection losses. Figure 2 illustrates the energy levels of different components in our solar cell. The reported values of LUMO of Sb_2S_3, CuSCN, and doped Spiro-OMETAD are 5.4, 5.3, and 5.2 eV. The barrier height decreases as the work function increases when the electrode contacts the p-type material [11]. Due to energy level alignment, excitons can be efficiently separated by the built-in electric field, transmitted to the surface layer and back layer, and collected by the corresponding electrodes. The HOMO and LUMO levels of TiO_2, Sb_2S_3, and HTMs increase gradually, which can improve the PCE. Since CuSCN/Spiro is better aligned compared to Spiro/CuSCN, this results in smooth charge transfer that reduces energy loss due to mismatched energy levels. Furthermore, a superior interface is formed by the CuSCN with the absorber layer, which leads to lower interfacial defect densities, then it helps to suppress non-radiative recombination and improves Voc and FF. This indicates that the efficiency in the CuSCN/Spiro configuration is higher compared to that in Spiro/CuSCN in our cells.

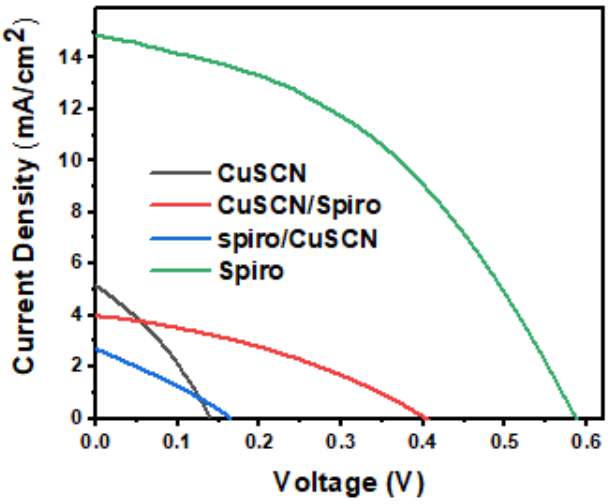

Figure 1: Current density-Voltage (J-V) curves of the devices with various configurations of HTMs

However, the FTO/Sb_2S_3/Spiro/Ag cell exhibits higher efficiency than FTO/TiO_2/Sb_2S_3/CuSCN/Spiro/Ag because the CuSCN surface is rough. The non-passivated interface introduces trap states, which can produce non-radiative recombination, leading to the low Voc compared to the spiro film.

Table 1: Photovoltaic parameters of the devices with various configurations of CuSCN and Spiro as HTMs

HTM	J_{SC} (mA cm^{-2})	V_{OC} (mV)	FF (%)	PCE (%)
CuSCN	5.01	136.8	33.2	0.23
CuSCN/Spiro	4.1	398.4	36.3	0.60
Spiro/CuSCN	2.7	161.0	29.5	0.13
Spiro	14.9	585.6	42.6	3.72

Table 2: The electronic properties of P3HT, Spiro-OMeTAD, and CuSCN [12, 13]

HTM	Energy gap (eV)	Conductivity (S cm^{-1})	Hole Mobility ($cm^2 V^{-1} S^{-1}$)	Hole Diffusion Co-efficient ($cm^2 s^{-1}$)
Spiro-OMeTAD	3.1	5.92×10^{-4}	2×10^{-5}	2.3
CuSCN	3.5	10^{-2}	1×10^{-1}	5.2×10^{-6}

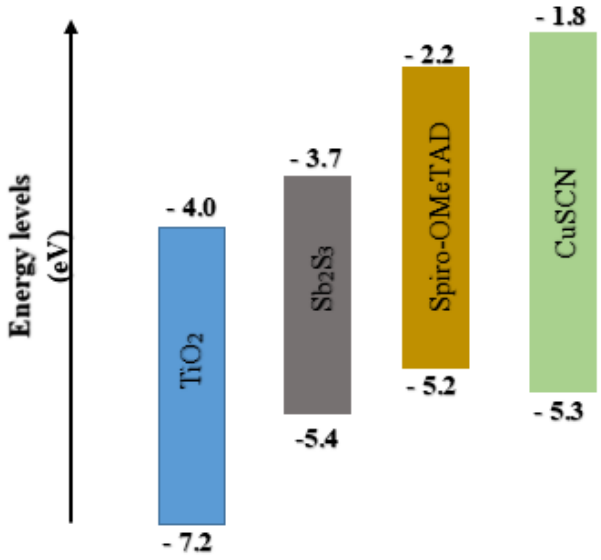

Figure 2: Schematic diagram of the energy levels of TiO_2, Sb_2S_3, Spiro-OMeTAD, and CuSCN

4.2 External Quantum Efficiency (EQE) measurement

The obtained IPCE spectra for the different configurations of HTMs are shown in Figure 3. The device with Spiro exhibits nearly 67% EQE, while the devices with CuSCN, CuSCN/spiro, and Spiro/CuSCN exhibit 20%, 15%, and 6%, respectively. These EQE responses align well with the Jsc values of the devices, which were obtained from J-V measurements. This spectrum indicates that charge collection in FTO/TiO_2/Sb_2S_3/Spiro/Ag is superior to that of the other configurations. Devices with a single layer of Spiro exhibited the

highest EQE spectral, consistent with superior Jsc. The single layer of CuSCN showed a strong and stable long- wavelength hole extraction due to optical transparency. Spiro on CuSCN showed a slight dip in the region of 400-600 nm. It can be due to the additional absorption or extraction loss at this combination. Because some of the incident light may have been absorbed by the HTL layers (CuSCN or Spiro) themselves, preventing those photons from reaching the Sb_2S_3 absorber and contributing to current. Spiro/CuSCN underperformed across all wavelengths, matching its high interfacial resistance.

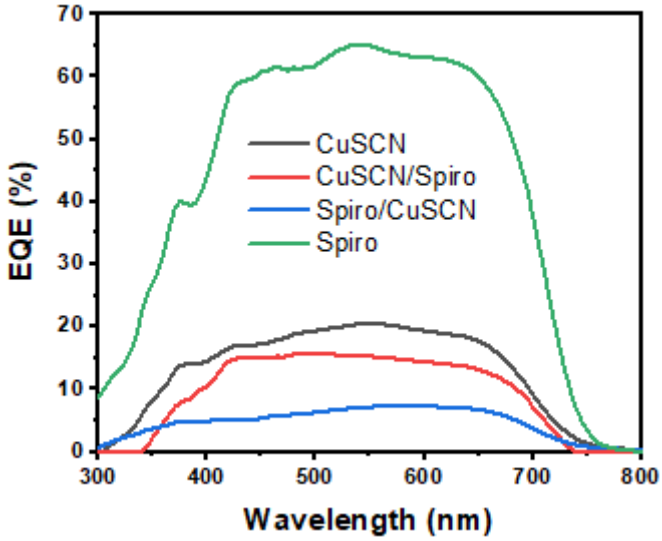

Figure 1: The EQE response curves of the devices with various configurations of HTM

4.3 Electrochemical Impedance Spectroscopy (EIS)

Figure 4 shows the EIS plot for the devices with different combinations of CuSCN and Spiro as HTM. The extracted impedance parameters from the fitting curves are listed in Table 3. The arc at high frequency corresponds to the hole transport. This hole transport affects FF, which contributes to the series resistance. The Rs represent the series resistance, while R_1 and R_2 are the charge transfer resistance at Sb_2S_3/HTM and TiO_2/Sb_2S_3.

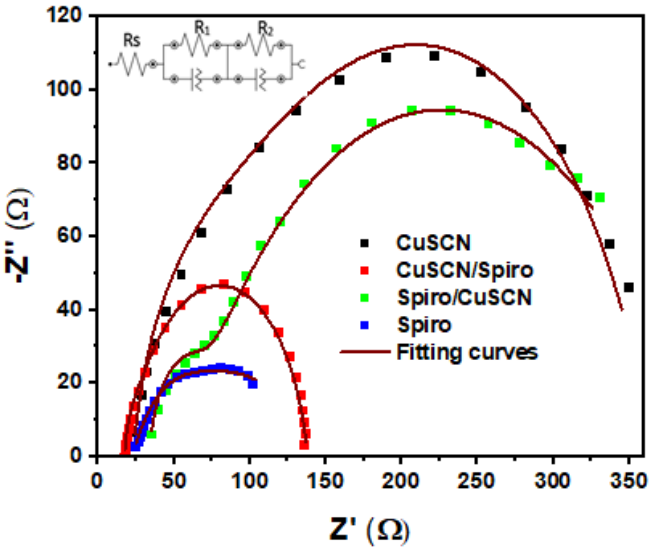

Figure 2: EIS plot with the equivalent circuit of the devices with various configurations of CuSCN and Spiro as HTMs

If the interface is not passivated well, it may introduce trap states**,** which increase non-radiative recombination**,** and the inhomogeneities create shunting paths or hinder complete coverage. This leads the charge transfer resistance. In the devices with CuSCN, the hole extraction is hard. Therefore, R_1 is considerably high in FTO/TiO_2/Sb_2S_3/CuSCN/Ag. Due to the recombination process at TiO_2/Sb_2S_3, the R_2 could be high. By introducing Spiro on CuSCN as HTM, the R_1 reduces because of the band alignment and the ability of hole transfer of Spiro. It reduces the R_S value too. But, for the device with Spiro/CuSCN as HTM, the band alignment with Sb_2S_3 is being interrupted. Therefore, the resistance is increasing. However, the device with Spiro as HTM shows very low R_1 compared to others, which could surpass the R_2 and R_S.

By comparing the R_2 values of the devices with CuSCN/Spiro and Spiro, the device with Spiro exhibits a higher value than CuSCN/Spiro. But the device with Spiro reveals a higher efficiency than CuSCN/Spiro. Because, after the separation of photogenerated carriers, they get recombined before reaching the selective contacts in CuSCN/Spiro.

Table 1: Impedance parameters of the devices with various configurations of CuSCN and Spiro as HTMs

HTM	Rs (Ω)	R_1 (Ω)	R_2 (Ω)
CuSCN	23.3	281	58.5
CuSCN/Spiro	17.6	115	6.07
Spiro/CuSCN	33.4	334	26.0
Spiro	22.0	99.2	22.5

5. Conclusion

This study systematically evaluated the performance of Sb_2S_3 solar cells employing various hole transport layers, including CuSCN and Spiro, and their combinations. Electrochemical Impedance Spectroscopy analysis revealed considerably less series resistance (Rs) and charge transfer resistances (Rct) for a single layer of spiro, which attributes the compactness of spiro as HTL. Spiro/CuSCN layer showed higher Rs and Rct compared to CuSCN/Spiro. The reduction of charge transfer resistance implies the mínimum recombination and efficient hole transfer. External quantum efficiency spectra aligned with Jsc trends and proved that the Spiro over CuSCN introduces an unfavourable interface morphology, leading to the losses. EQE of a single CuSCN showed a stable performance. Our findings indicate that the sequence of HTL deposition significantly influences device efficiency. Device employing Spiro as the HTL achieved the highest power conversion efficiency attributed to its favourable energy level alignment, especially interfacial connection and efficient hole extraction capabilities. The CuSCN configuration exhibited intermediate performance, suggesting that the sequence of a HTL deposition influences both charge transport and interfacial interactions.

.

References

1. Martin A. Green. (2019). The Path to 25% Silicon Solar Cell Efficiency: History of Silicon Cell Evolution. *Prog. Photovolt: Res. Appl.*, 17:183–189.
2. Jason Svarc. (2025). Most efficient solar panels 2025. Retrieved March 20, 2025.
3. NREL transforming energy, Best Research Cell Efficiencies. 2025 [online] Available at: https://www.nrel.gov/pv/interactive-cell-efficiency.html [Accessed 18 June 2025].
4. Rombach, F.M., Haque, S. A., Macdonald, T.J. (2021). Lessons learned from spiro-OMeTAD and PTAA in perovskite solar cells. *Energy & Environmental Science*.
5. Li, G., et al. (2022). Inhibited Aggregation of Lithium Salt in Spiro-OMeTAD for Perovskite Solar Cells. *Crystals*, 12(2), 290.
6. Chen, J., Park, N.G. (2018). Inorganic hole transporting materials for stable and high efficiency perovskite solar cells. *The Journal of Physical Chemistry C*, 122(25), 14039-14063.
7. Matebese, F., Taziwa, R., Mutukwa, D. (2018). Progress on the synthesis and application of CuSCN inorganic hole transport material in perovskite solar cells. *Materials* 11(12), 2592.
8. Syed Zulqarnain Haider, Hafeez Anwar, and Mingqing Wang. (2019). Theoretical Device Engineering for High-Performance 2 Perovskite Solar Cells Using CuSCN as Hole Transport Material Boost the Efficiency Above 25%. Phys. *Status Solidi A*, 1900102.
9. O'Regan B., Lenzmann F., Muis R., A. (2002). solid-state dyesensitized solar cell fabricated with pressure-treated P25-TiO_2 and CuSCN: Analysis of pore filling and IV characteristics. *Chem. Mater.*, 12, 5023–5029.
10. Christians, J.A., Kamat, P.V., (2013). Trap and transfer. Two-step hole injection across the Sb_2S_3/CuSCN interface in solid-state solar cells. *Acs Nano* 7(9), 7967-7974.
11. Feng, P., et al. (2010). Nonvolatile resistive switching memories-characteristics, mechanisms and challenges. *Progress in Natural Science:* Materials International 20, 1-15.
12. Jiménez-López, J., et al. (2017). Charge injection, carriers recombination and HOMO energy level relationship in perovskite solar cells. *Scientific reports* 7(1), 1-10.
13. Madhavan, V.E., et al. (2019). CuSCN as hole transport material with 3D/2D perovskite solar cells. *ACS Applied Energy Materials* 3(1), 114-121.